Available online at www.sciencedirect.com

ScienceDirect

Procedia CIRP 104 (2021) 875–880

www.elsevier.com/locate/procedia

54th CIRP Conference on Manufacturing Systems

Finite element modelling of temperature in cylindrical grinding for future integration in a digital twin

Arttu Heininen*[a], Romaric Prod'hon[a], Hossein Mokhtarian[a], Eric Coatanéa[a], Kari Koskinen[a],

[a]*Tampere University, Korkeakoulunkatu 7, Tampere 33720, Finland*

* Corresponding author. Tel.: +358-50-301-3973; *E-mail address:* arttu.heininen@tuni.fi

Abstract

This paper focuses on finite element modelling of temperature field in cylindrical grinding. The developed model is validated against two established and validated thermal models in cylindrical grinding. The models' results are compared in terms of suitability for a digital twin application. The computation time requirement for a real-time temperature estimator in grinding digital twin is defined. The FEM model offers the most fidelity, but computational demands prevent its use in a digital twin. Therefore, the need for coupling the FEM model with an AI-based approaches for future work is highlighted to achieve temperature estimation within the wheel contact time.

Keywords: Grinding; Digital twin; Finite element method; Contact length

1. Introduction

Digital Twin (DT) technology has been one of the leading research topics in manufacturing sector in the recent years [1]. A DT is a fusion of a physical entity (e.g. product, manufacturing machine), virtual entity (model), and bi-directional data connection between the physical and virtual entities. The virtual entity aims to mirror the physical entity through data inputs from sensors, expert knowledge, and models describing the behaviour of the physical entity. Through a feedback process, the virtual entity provides the possibility to interact with the machine settings in real-time [2]. Researchers have highlighted the use of surrogate models in DT development [2, 3]. The real-time aspect of DT requires that data acquisition, model computation, and analysis must be quasi-instantaneous. The main goal of implementing DT in manufacturing is to ensure part quality while reducing the cost [4]. Furthermore, DT enables to understand the behavior process through simulation and data analysis, predict part quality, and anticipate part defect. The ability of DT to run virtual experiments prior to the real experiments, reduces the experimental effort and the overall costs. Development of DT is particularly crucial for the end-processes that determine the final quality of parts such as grinding.

Desired surface roughness and dimensional accuracy of workpiece are often achieved by grinding operations. Despite the long-term use of grinding in manufacturing, its productivity and repeatability are limited by remaining challenges such as thermal damages, material phase changes, and tensile residual stress. Implementing DT in grinding process aims at tackling these aforementioned challenges by using computationally efficient modelling and data analysis. More specifically, a DT in grinding must integrate models operating on both microscopic and macroscopic scales, empirical laws resulting from experiments, simulations results and experimental data.

Finite Element Method (FEM) allows to simulate the process in different spatial and temporal scales. For instance, the temperature field time history is modelled by the heat equation that describes the temperature diffusion process. In addition to models described above, DT utilises experimental data derived from Barkhausen noise measurements [5], acoustic emission signals [6], grinding power [7], forces and temperature distributions [8] for example.

In grinding, the temperature management is crucial to ensure part quality [9]. High temperature in the workpiece during grinding induces tensile residual stresses, which affects the fatigue-life of the workpiece [10]. Residual stresses are typically controlled offline using non-destructive methods like Barkhausen noise [5].

Temperature measurements can be performed on-line, but this is challenging in wet grinding [8]. The measurement is typically done using thermocouples or thermal infrared cameras.

10.1016/j.procir.2021.11.147

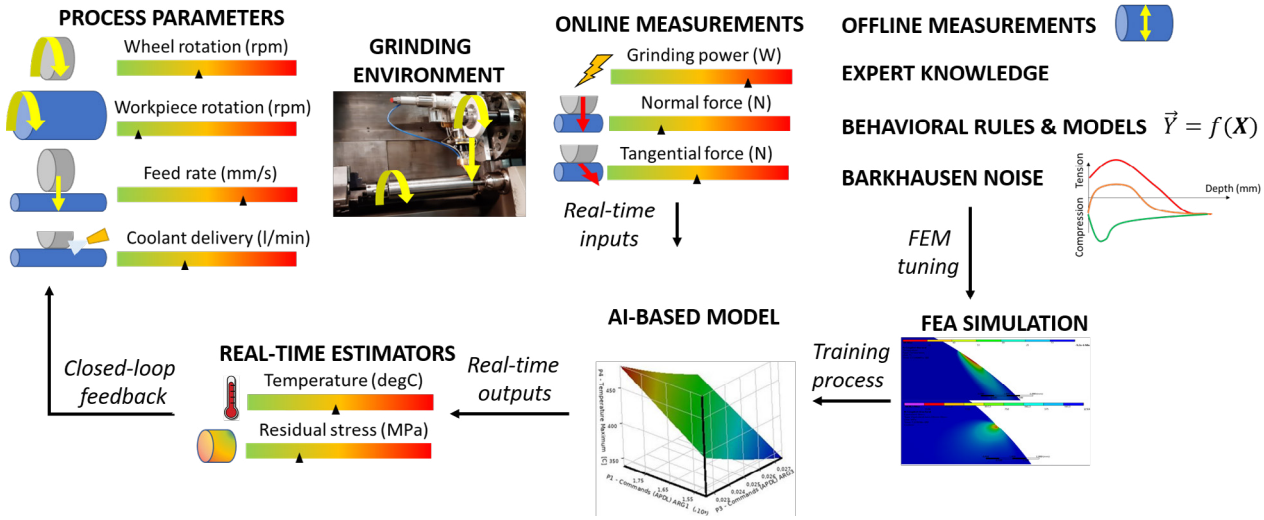

Fig. 1. The architecture of the DT in grinding process.

Radiation-based measurements can be disrupted by the presence of coolant. These measurement approaches are incapable of capturing temperature within the contact area. Indirect measurement of other parameters is an alternative to direct temperature measurement. These measurements can be linked to thermal models providing the grinding temperature. Different models from analytical equations [11, 12] to numerical methods [13, 14] have been used to model grinding temperatures.

Grinding power is the main parameter considered for building a temperature model which can be measured using a Hall effect sensor. The response time of this type of sensor is around 0.5 μs [7]. This response time allows to reach typical acquisition frequencies of several kilohertz. Hence, the key challenge for an efficient real-time DT in grinding is to obtain models' response times within the same order of the sensor acquisition frequency. Such DT requires to integrate models that are computationally efficient. This is critical for DT versatility.

Power measurement with high acquisition rate and precision are conveniently possible. Due to challenges in temperature measurement, developing a real-time temperature estimator that computes temperature based on power online measurement data is essential for the real-time DT. The real-time estimator and its connection to the DT is shown in Fig. 1.

The research objective of the paper is to develop a temperature estimator which enables computing the whole temperature field based on measured power during the process for cylindrical grinding. Toward this end, our approach is to develop a FEM model, validate it with the well-established equations for calculating grinding temperature. Computing the whole temperature field is of importance for further modelling of residual stress. The developed model can be also used to create synthetic data for train further AI models. The remainder of this paper is organised as follows. In section 2, the governing equations describing the grinding parameters and their interactions are defined. Then two well-known thermal models are presented, namely, Jaeger's analytical model [15] and the maximum temperature approximation (MTA) model [9]. In section 3, FEM-based thermal model is developed to model the temperature field. The results of finite element model are compared with the two aforementioned models using a design of experiment (DOE). The research objective sought by the authors in this paper is to compare these three models in terms of computation time, and consistency in predicted temperature values. Section 4 describes the results of this study as well as ongoing developments. The conclusion summarises the contribution of this paper and highlights the benefits of coupling FEM and AI for future works.

2. Grinding models

2.1. Governing equations in cylindrical grinding

In external cylindrical grinding the wheel diameter d_s (m) and the workpiece diameter d_w (m) can be combined into the equivalent diameter, shown in equation 1. The sign in the denominator depends on the grinding process. A plus sign is used for external grinding and minus sign for internal grinding.

$$d_e = \frac{d_s.d_w}{d_s \pm d_w} \tag{1}$$

The geometrical contact length is defined as:

$$l_g = \sqrt{a_e.d_e} \tag{2}$$

where a_e (m) represents the depth of cut. It has been shown by inverse heat transfer analysis that l_g underestimates grinding contact length [16]. Indeed, the force exerted by the grinding wheel is causing deflections which increases the real contact length. The normal force F_n is also related to the grinding power P. Thus, a model for assessing deflected contact length l_f (equation 3) has been developed that matches better with experimental temperature measurements [17].

$$l_f = \sqrt{\frac{8.R_r^2.F_n.d_e}{\pi.b_w.E^*}} = \sqrt{\frac{8.R_r^2.P.d_e}{\pi.\mu.v_s.b_w.E^*}} \tag{3}$$

Here R_r is the dimensionless roughness factor which depends on the grinding contact conditions (dry or wet grinding), b_w (m) is the grinding wheel width. F_n (N) is the normal force, μ is the grinding coefficient analogous to a friction coefficient, v_s (m/s) is the grinding wheel peripheral speed, and P (W) the grinding power which could be measured online. E^* (Pa) is the combined Young's modulus, defined as:

$$\frac{1}{E^*} = \frac{1-\nu_s^2}{E_s} + \frac{1-\nu_w^2}{E_w} \tag{4}$$

where ν_s and ν_w are the wheel and workpiece Poisson's ratios, and E_s and E_w are the corresponding Young's moduli.

The total contact length l_c in then defined by the combined contribution of geometrical contact length l_g and deflected contact length l_f according to equation 5:

$$l_c = \sqrt{l_g^2 + l_f^2} \tag{5}$$

Based on the total contact length l_c, the average heat flux q_w is calculated with equation 6 which represents the heat transferred to the part on the contact zone as a function of the grinding power P. Here ϵ is the ratio between the heat transferred to the workpiece and the total heat.

$$q_w = \frac{\epsilon.P}{l_c.b_w} \tag{6}$$

2.2. Thermal models

2.2.1. Jaeger's analytical model

A well established thermal model used in grinding temperature modelling is Jaeger's analytical model [15]. In the model, the actual interaction between the wheel and the workpiece is replaced by applying a moving heat flux on the workpiece surface. The integral equation is given in [12] as:

$$T = \int_0^{l_c} \frac{q}{\pi k_w} exp\left[\frac{v_w(x-\zeta)}{2\alpha_w}\right] K_0\left\{\frac{v_w\sqrt{(x-\zeta)^2+z^2}}{2\alpha_w}\right\} d\zeta \tag{7}$$

where α_w (m^2/s) is the thermal diffusivity of the workpiece, k_w ($W.m^{-1}.K^{-1}$) is the thermal conductivity of the workpiece, K_0 is the zeroth order modified Bessel function of the second kind. The positive z (m) coordinate is in the opposing direction of the outward normal of the workpiece surface. The positive x (m) coordinate is perpendicular to z. $\zeta \in [0, l_c]$ is a dummy variable of integration, whose origin is placed on the start of the contact length shown in Fig. 2. It also shows the relative velocity, V_{rel}, (in this case V_{rel}=v_s-v_w) between the workpiece and the grinding wheel and the direction of the heat flux. The heat flux distribution q is modeled using a right-angled triangular distribution [14, 9]:

$$q = 2.q_w\left(\frac{\zeta}{l_c}\right) \tag{8}$$

where q_w is calculated using eq. (6). The model is based on quasi-stationary condition, which states that the workpiece must be long enough compared to the heat penetration depth. Also, the velocity of the moving heat source must be sufficiently fast compared to the heat conduction in the direction of motion. This condition is fulfilled if the Peclet number, L given in Equation 9, is greater than 5 [9]:

$$L = \frac{v_W.l_c}{4.\alpha_w} \tag{9}$$

In this model, temperature change for a point far from heat source is zero.

Considering these assumptions, the model is only valid for a workpiece whose dimensions are large compared to the heat source size. Secondly, the model is not valid near material boundaries (e.g. corners, ends). Thirdly, the workpiece peripheral velocity must be large enough for the quasi-stationary condition to apply. Also, the model does not consider cooling by the coolant and considers temperature-independent material properties producing a temperature-dependent error in the estimated temperature field. In reality, the thermal conductivity k_w and the thermal diffusivity α_w are functions of the workpiece temperature. Jaeger's model provides the whole temperature field and is not computationally demanding compared to numerical methods like FEM. The accuracy of the produced temperature field increases with the amount of space sampling points (x,z). High amount of sampling points is required for further modelling of residual stresses. This increases the computation time, which is limited by the model requirement to operate in a real-time system.

2.2.2. Maximum temperature approximation (MTA)

The second model considers the maximum temperature [11] given by Jaeger's model (equation 7):

$$T_m = \frac{1.06.q_w.\alpha_w^{1/2}.l_c^{1/2}}{k_w.v_w^{1/2}} \tag{10}$$

This model depends on the shape of the assumed heat flux distribution. The constant 1.06 is valid for a triangular distribution shown in Fig 2 and changes with another heat flux distribution.

The limitations of Jaeger's model applies also to this model. In addition, MTA model only provides the maximum temperature and not the whole temperature field. However, its simplicity allows fast analysis of the effect of chosen process parameters on the temperature. MTA model is fast enough to be computed in real-time, since response time is in the order of milliseconds.

2.3. Computation time considerations

The wheel contact time t_s (s) given by equation (11) is the time that a given point on the workpiece surface travels across the contact length.

$$t_s = \frac{l_c}{v_w} \tag{11}$$

The grain contact time, t_g (s), given by equation (12) is the time for an abrasive grain to travel across the contact length.

$$t_g = \frac{l_c}{v_s} \tag{12}$$

The grain contact time t_g is significantly shorter than the wheel contact time t_s. Typical orders of magnitude for these two variables are 5 ms for t_s and 30 μs for t_g [17]. In other words, t_g is operating on a microscopic timescale which is not compatible with acquisition frequencies of Hall effect sensor [7]. Thus, controlling the process at the grain level is infeasible. However, controlling the process at macroscopic timescale is feasible due to the order of magnitude of t_s. Therefore, the computation time of temperature estimator in DT should consider these time constraints. Indeed, the results of the temperature estimator (whole temperature field) should be obtained within the wheel contact time t_s to get a fully operating real-time estimator. This limits the possible modelling methods and highlights the interest of using fast prediction methods, as discussed in the future perspective of this research.

3. Finite Element Model Implementation

The FEM Model developed in this section, considers a moving heat source of length l_c (m) moving with a constant velocity v_w (m/s) on the surface of the cylindrical workpiece of with the diameter of d_w (m) as shown in Fig. 2. The workpiece diameter in this study is 29 mm and the material is steel 55NiCrMoV7. The governing differential equation for the heat conduction within the workpiece Ω, is described as [18]:

$$\rho c_w \frac{\partial T}{\partial t} = -k\Delta T \quad in\ \Omega, t > 0 \tag{13}$$

where c_w $(J.kg^{-1}.K^{-1})$ is the workpiece specific heat capacity. The initial condition is given as:

$$T(x, y, t) = T_0 \quad in\ \Omega, t = 0 \tag{14}$$

where T_0 (K) is the initial temperature of the workpiece considered to be uniform. At a specific time, the heat source is present on the section Γ_1 of the workpiece surface as shown in Fig. 2. This is the first boundary condition for the governing differential equation, and it is described as:

$$k\left(\frac{\partial T}{\partial n}\right) = q \quad in\ \Gamma_1,\ t > 0 \tag{15}$$

where n is the unit normal vector pointing outwards of the surface of the workpiece.

The second boundary condition describes the cooling of the workpiece by the surrounding air which occurs on the section Γ_2 of the workpiece surface as shown in Fig. 2:

$$-k\left(\frac{\partial T}{\partial n}\right) = h_{air}(T - T_{ref}) \quad in\ \Gamma_2,\ t > 0 \tag{16}$$

where T_{ref} (K) is the reference temperature of the external environment. h_{air} is the air heat transfer coefficient $(W.m^{-2}.K^{-1})$ which is solved from:

$$h_{air} = \frac{\overline{Nu} k_{air}}{d_w} \tag{17}$$

where k_{air} $(W.m^{-1}.K^{-1})$ is the air heat conductivity, d_w (m) is the workpiece diameter, and Nu is the average Nusselt number.

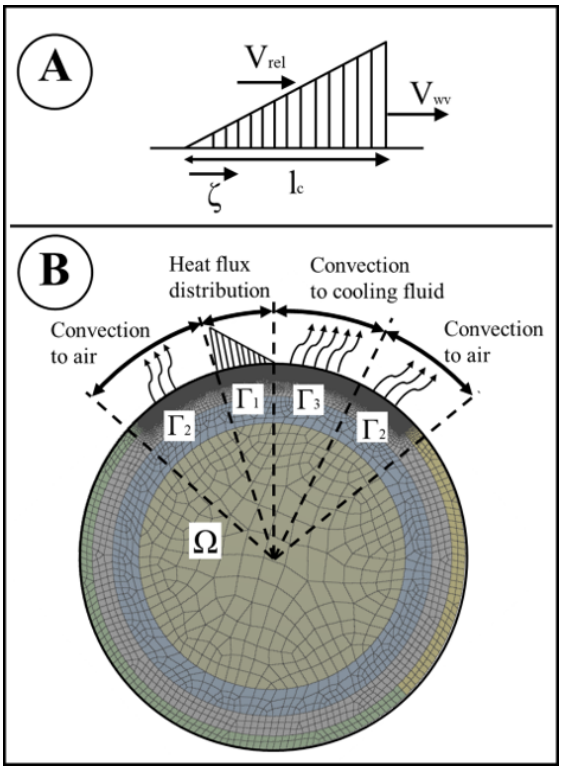

Fig. 2. A: Triangular heat flux distribution / B: Mesh considerations and defined boundary condition in the FEM model

For a rotating cylinder, an average value of the Nusselt number is given by [18]:

$$\overline{Nu} = 0.133.Re^{2/3}.Pr^{1/3};$$
$$Re < 4.3e5,\ 0.7 < Pr < 670. \tag{18}$$

Re is the Reynolds number

$$Re = \frac{v_w.d_w}{\nu_{air}} \tag{19}$$

where v_w (m/s) is the workpiece peripheral speed mentioned above and d_w (m) is the workpiece diameter. ν_{air} $(m^2.s^{-1})$ is the air kinematic viscosity. In equation 18, Pr is the air Prandtl number (0.71 at room temperature).

The third boundary condition describes the cooling effect of the coolant on the workpiece which occurs on the section Γ_3 of the workpiece surface as shown in Fig. 2:

$$-k\left(\frac{\partial T}{\partial n}\right) = h_f(T - T_{ref}) \quad in\ \Gamma_3,\ t > 0 \tag{20}$$

where h_f $(W.m^{-2}.K^{-1})$ is the coolant heat transfer coefficient, which is estimated using fluid wheel model [17]:

$$h_f = \frac{\beta_f}{C}\sqrt{\frac{v_s}{l_c}} \tag{21}$$

where β_f is the fluid thermal effusivity:

$$\beta_f = \sqrt{k_f \rho_f c_f} \tag{22}$$

where k_f ($W.m^{-1}.K^{-1}$) is the fluid thermal conductivity, ρ_f (kg/m^3) is density, and c_f ($J.kg^{-1}.K^{-1}$) its specific heat capacity. In equation 21, C is a constant depending on the shape of the heat source, the contact angle and the Peclet number.

The governing equation 13 is presented in a matrix form:

$$\mathbf{C}(T)\mathbf{T}'(t) + \mathbf{K}(T)\mathbf{T}(t) = \mathbf{Q}(t) \tag{23}$$

where **C** and **K** are the specific heat and conductivity matrices, **T** is the nodal temperature vector and **T'** its time derivative, and **Q** is the vector of nodal heat flow. Solving the matrix equations using FEM gives temperature field at each time step. For each consecutive time step the heat source moves and the boundary conditions are updated. The time step dt depends on the element size, and at least 30 elements should be present within the contact length [14]:

$$dt = \frac{element\ size}{v_{wp}} \tag{24}$$

For a single pass of the grinding wheel, the maximum temperature reaches a quasi-steady state [9]. This allows to simulate only a portion of the full workpiece. Starting from zero rotating angle, the heat source moves on the surface of the workpiece until a 90-degree angle was reached.

The workpiece cross-section was modelled using 8-node quadrilateral elements using non-linear shape functions. As the temperature gradients are large near the surface, a dense element distribution was used (see Fig. 2). The total number of nodes was 185908 for this workpiece. The mesh independence was achieved by starting with a coarse mesh, which was refined by halving the element size near the surface, until the maximum temperature was less than 2% between successive refinements. The FEM model is implemented in ANSYS software.

An important advantage of the FEM model is that it produces the whole temperature field considering the cooling and possible complex geometry. Computing the whole temperature field is crucial because it is a prerequisite for modelling residual stress in grinding. In addition, its validity is not limited by the workpiece dimensions or line source velocity. Furthermore, by solving the transient heat equation, time-history of the temperature field is obtained. The FEM model allows to consider the use of time-dependent heat flux. The FEM model is not quasi-stationary like Jaeger's model is. However, computational time is its main weakness for using in a DT.

4. Results

The objective of this section is to compare the consistency of developed FEM model with the existing Jaeger's and MTA models for grinding temperature approximation. A full factorial DOE was used to compare the maximum temperature predicted by the models. Three influencing parameters with three levels each were chosen for the DOE, namely, grinding wheel peripheral velocity v_s (30, 40, and 50 m/s), grinding power P (1, 2, and 3 kW), and depth of cut a_e (6, 12, 24 μm). Note that the grinding power results from the interaction of the grinding grains and workpiece. In other words, grinding power is not among grinding parameter settings, but it is influenced by the parameter settings. Since grinding power is a measurable parameter, it can be used as an input for the thermal models, instead of considering all other parameter settings and grinding conditions. Table 1 shows the resultant maximum temperature T_{max} computed by MAT, Jaeger's model, and FEM model as well as the relative difference between these models. Jaeger's model predicts lower temperatures and MTA higher temperatures than the FEM model. The maximum relative difference (RD) of 2.9% and 4% for MTA and Jaeger's model validates the consistency of the developed FEM with existing models.

Table 1. A Design of experiments comparing maximum temperature computed by FEM model with MAT and Jaeger's model by relative difference (RD)

	Inputs			T_{max}	RD	RD
#	a_e	P	v_s	FEM	MTA/FEM	Jaeger/FEM
	(μm)	(W)	(m/s)	($^\circ C$)	(%)	(%)
1	6	1000	30	152.8	1.5	-2.8
2	6	1000	40	161.7	2.3	-1.8
3	6	1000	50	168.9	2.9	-1.1
4	6	2000	30	260.3	1.4	-3.5
5	6	2000	40	277.0	2	-2.7
6	6	2000	50	290.2	2.5	-1.9
7	6	3000	30	353.9	1.4	-3.9
8	6	3000	40	376.6	2.2	-2.9
9	6	3000	50	395.2	2.7	-2.1
10	12	1000	30	149.7	1.4	-2.9
11	12	1000	40	157.6	2.2	-2.0
12	12	1000	50	163.9	2.6	-1.5
13	12	2000	30	257.5	1.3	-3.6
14	12	2000	40	273.2	1.9	-2.8
15	12	2000	50	285.3	2.4	-2.1
16	12	3000	30	350.7	1.6	-3.8
17	12	3000	40	372.8	2.2	-2.9
18	12	3000	50	390.7	2.6	-2.3
19	24	1000	30	144.6	1.1	-3.3
20	24	1000	40	151.3	1.6	-2.7
21	24	1000	50	156.1	2.0	-2.2
22	24	2000	30	252.6	1.1	-3.9
23	24	2000	40	266.3	1.7	-3.1
24	24	2000	50	277.2	2.0	-2.6
25	24	3000	30	346.1	1.4	-4
26	24	3000	40	366.7	1.9	-3.2
27	24	3000	50	382.4	2.4	-2.6

Each model's advantages and weaknesses are discussed in their corresponding sections (section 2, section 3) and summarised in Table 2. The whole temperature field can be obtained by using Jaeger's and FEM models. However, the required computation time is longer than the wheel contact time t_s (section 2.3). Thus, the integration of these models into a real-time digital twin is infeasible. On the other hand, the MTA model provides only the maximum temperature within the contact time t_s.

According to Table 2, the FEM model provides the best fidelity, but it lacks computation time efficiency for being integrated in a real-time DT. The comparison of the thermal models

in this article highlights the need to have a thermal model which provides the whole temperature field in real-time. Computing the whole temperature field is required to model more complex phenomena such as thermo-mechanically induced residual stress. Residual stresses are still a key challenge is grinding.

Table 2. Qualitative comparison of the thermal models

Pros/Cons	FEM	Jaeger	MTA
Whole field	✓	✓	✗
Time history	✓	✗	✗
Cooling	✓	✗	✗
T-dependent properties	✓	✗	✗
Complex geometries	✓	✗	✗
Real-time	✗	✗	✓

5. Conclusion and perspective

In this paper, a FEM model is developed to predict temperature field for cylindrical grinding. The FEM model was validated by comparing the results with existing analytical models using a full factorial DOE. The FEM model computes the whole temperature field with a high fidelity making it suitable for an integration in a digital twin and further modelling of thermo-mechanical residual stress. It was discussed that the computation time of the thermal model must be within the wheel contact time (in the order of milliseconds) to be considered in a real-time digital twin for grinding. Nevertheless, the FEM model is computationally demanding and consequently time consuming for typical computers, which is a barrier for a real-time DT. Therefore, computation time is a key challenge in integrating FEM models in a real-time DT. The time efficiency is needed to ensure proper integration of available online sensors data.

A second limitation of the present approach is the level of integration of the mechanical phenomena in the current FEM model. The model is currently limited to the thermal modelling. Integrating thermo-mechanical phenomena to assess residual stress is needed since thermo-mechanical residual stresses play a significant role in the grinding process. This aspect will be the scope of future developments of the FEM model presented in this study.

Among the possible perspectives, the coupling of Artificial Intelligence approaches could be considered to combine both the FEM model fidelity and the rapidity of prediction of AI approaches. For instance, an Artificial Neural Network could learn the relationship between the grinding parameters and the temperature field and predict the temperature field online within a short response time. An appealing approach is to use the thermo-mechanical model to generate synthetic datasets that will be used to train the AI-model.

As a summary, the paper contribution has been the development and validation of a FEM-based thermal model used for future integration in a grinding digital twin. It has been shown that the FEM model cannot be used as such for real-time prediction in DT. However, the FEM model can be used to generate synthetic data used for training AI models. The FEM model is then coupled with AI and is a powerful and versatile tool to tackle complex phenomena (complex geometries, temperature-dependent material properties, cooling effects, time-history). This research is an on-going research and it should further be developed into the integration of a FEM model into a real-time digital presentation of the grinding process allowing thermal control of the grinding process.

Acknowledgements

The support of ÄVE-project and Business Finland in making this research possible is greatly acknowledged.

References

[1] Jones, D., Snider, C., Nassehi, A., Yon, J., & Hicks, B. (2020), Characterising the Digital Twin: A systematic literature review. CIRP Journal of Manufacturing Science and Technology.
[2] Chakraborty, S., Sondipon, A., Ranjan, G., 2020. The role of surrogate models in the development of digital twins of dynamic systems, Applied mathematical modeling 90, 662-681.
[3] Waxenegger-Wilfing, G., Dresia, K., Deeken, J., Oschwald, M., 2020 Heat Transfer Prediction for Methane in Regenerative Cooling Channels with Neural Networks, Journal of Thermophysics and Heat Transfer, 34(2), 347-357.
[4] Kritzinger, W., Karner, M., Traar, G., Henjes, J., & Sihn, W. (2018). Digital Twin in manufacturing: A categorical literature review and classification. IFAC-PapersOnLine, 51(11), 1016-1022.
[5] Neslušan, M., Čížek, J., Kolařík, K., Minárik, P., Čilliková, M., & Melikhova, O. (2017). Monitoring of grinding burn via Barkhausen noise emission in case-hardened steel in large-bearing production. Journal of Materials Processing Technology, 240, 104-117.
[6] Liu, Q., Chen, X., & Gindy, N. (2006). Investigation of acoustic emission signals under a simulative environment of grinding burn. International Journal of Machine Tools and Manufacture, 46(3-4), 284-292.
[7] Kwak, J. S., Sim, S. B., & Jeong, Y. D. (2006). An analysis of grinding power and surface roughness in external cylindrical grinding of hardened SCM440 steel using the response surface method. International journal of machine tools and manufacture, 46(3-4), 304-312.
[8] Batako, A. D., Rowe, W. B., & Morgan, M. N. (2005). Temperature measurement in high efficiency deep grinding. International journal of machine tools and manufacture, 45(11), 1231-1245.
[9] Malkin, S., Guo, C., 2007. Thermal analysis of grinding, Cirp annals 56.2, 760-782.
[10] Ding, W., Zhang, L., Li, Z., Zhu, Y., Su, H., Xu, J., 2017. Review on grinding-induced residual stresses in metallic materials, International Journal of Advanced Manufacturing Technology 88, 2939-2968.
[11] Malkin, S., & Guo, C. (2008). Grinding technology: theory and application of machining with abrasives. Industrial Press Inc..
[12] Rowe, W. B. (2001). Thermal analysis of high efficiency deep grinding. International Journal of Machine Tools and Manufacture, 41(1), 1-19.
[13] Guo, C., & Malkin, S. (2000). Energy partition and cooling during grinding. Journal of Manufacturing Processes, 2(3), 151-157.
[14] Anderson, D., Warketi, A., Bauer, R., 2008. Experimental validation of numerical thermal models for dry grinding, Journal of materials processing technology 204, 269-278.
[15] Carslaw, H. S., Jaeger, J. C. (1959). Conduction of heat in solids. Clarendon P.
[16] Rowe, W. B., Black, S. C. E., Mills, B., Qi, H. S., & Morgan, M. N. (1995). Experimental investigation of heat transfer in grinding. CIRP Annals Manufacturing Technology, 44(1), 329-332.
[17] Rowe, W. B. (2013). Principles of modern grinding technology. William Andrew.
[18] Mills, A., F., (1999), Basic heat and mass transfer, Prentice hall.
[19] Mahdi, M., & Zhang, L. (1998). Applied mechanics in grinding—VI. Residual stresses and surface hardening by coupled thermo-plasticity and phase transformation. International Journal of Machine Tools and Manufacture, 38(10-11), 1289-1304.